Brittle to Ductile Transition in a Fiber Bundle with Strong Heterogeneity

Kornél Kovács
Department of Theoretical Physics, University of Debrecen, P. O. Box: 5, H-4010 Debrecen, Hungary

Raul Cruz Hidalgo
Departamento de Fısica, Facultad de Ciencias, Universidad de Navarra, 31080 Pamplona, Spain

Ignacio Pagonabarraga
Departament de Física Fonamental, Universitat de Barcelona, Carrer Martí i Franqués 1, E-08028 Barcelona, Spain

Ferenc Kun*
Department of Theoretical Physics, University of Debrecen, P. O. Box: 5, H-4010 Debrecen, Hungary
(Dated: September 5, 2012)

We analyze the failure process of a two-component system with widely different fracture strength in the framework of a fiber bundle model with localized load sharing. A fraction $0 \leq \alpha \leq 1$ of the bundle is strong represented by unbreakable fibers, while fibers of the weak component have randomly distributed failure strength. Computer simulations revealed that there exists a critical composition α_c which separates two qualitatively different behaviours: below the critical point the failure of the bundle is brittle characterized by a catastrophic collapse, however, above α_c the macroscopic response becomes ductile providing stability during the entire breaking process. The transition occurs at an astonishingly low fraction of strong fibers which can have importance for applications. We show that in the ductile phase the size distribution of breaking bursts has a power law functional form with an exponent 2 followed by an exponential cutoff. In the brittle phase the power law prevails, however, with a higher exponent 9/2. The transition between the two phases proved to be analogous to continuous phase transitions. Analyzing the microstructure of damage it was found that at the beginning of the fracture process cracks nucleate randomly, while later on growth and coalescence of cracks dominate giving rise to power law distributed crack sizes.

PACS numbers: 05.90+m, 81.40.Np

I. INTRODUCTION

Beyond its engineering relevance, the complexity of the fracture of brittle and ductile materials is of great interest for physics and materials science, as well. Recently, the application of statistical physics has revealed interesting novel aspects of the damage and fracture of heterogeneous materials increasing our understanding both on the micro and macro scales of fracture processes [1]. Most of these theoretical investigations relay on mesoscopic discrete models such as fiber bundles [2–5] and lattices of fuses [6, 7], springs, or beams [8–10], where disorder is typically captured by the random strength of elements. Analytic calculations and computer simulations have revealed that for a broad class of disorder distributions the fracture of heterogeneous materials exhibit universal aspects both on the micro- and macro level: the size of bursts has a power law distribution with universal exponents [3–5, 11, 12], furthermore, macroscopic failure occurs in the form of localization after a precursory sequence of microcracking [13–15]. Interesting analogies have been established between the failure of materials and phase transitions and critical phenomena [15–19].

However, real materials are often of composite nature, *i.e.* they have two or more components with widely different properties which provide an improved fracture toughness. For instance, in fiber reinforced composites where fibers are embedded in a carrier matrix, the matrix material typically has much lower fracture strength than the fibers. This widely different strength of the components combined with appropriate coupling results in an improved damage tolerance which has a high relevance for applications [20]. It has been shown that in heterogeneous materials varying the local mechanical response and of the amount of disorder of the components one can achieve a transition from brittle to quasi-brittle or even to ductile failure [21–24].

In this paper we study the effect of strong heterogeneity on the fracture process of disordered materials based on a fiber bundle model with localized interaction. Our model is composed of two subsets of fibers with widely different fracture behavior: fibers of one of the subsets are strong in the sense that they can support any load and never break, while fibers of the other type are weak characterized by a probability distribution of failure strength. The two components form a homogeneous mixture on a square lattice with periodic boundary conditions in both directions. It is a crucial element of our approach that after failure events the load of broken fibers is equally

*Email address:ferenc.kun@science.unideb.hu

redistributed solely over their intact nearest neighbors leading to high stress concentration around failed regions. Such localized load sharing systems are known to be very brittle, however, our investigations demonstrate that the presence of strong fibers moderates the effect of stress inhomogeneities and leads to a ductile macroscopic response when exceeding a critical fraction. We explore by computer simulations how the brittle-ductile transition occurs on the microscale by investigating the size distribution of bursts and the microstructure of damage.

II. MIXTURE OF WEAK AND STRONG FIBERS

We consider a parallel bundle of fibers organized on a square lattice of size L. Under an increasing external load the fibers present a linearly elastic behavior characterized by the same Young modulus E. To model the two-component mixture, a fraction $0 \leq \alpha \leq 1$ of the $N = L^2$ fibers of the lattice is considered to be unbreakable, *i.e.* they can support any load without failure. These strong fibers of number $N_S = \alpha \cdot N$ are distributed randomly all over the lattice without any spatial correlations. The remaining $1-\alpha$ fraction of fibers of number $N_W = (1-\alpha)N$ are considered to be weak, i.e. they have only a finite load bearing capacity and break when the local load on them exceeds their failure threshold. The breaking thresholds of weak fibers σ_{th}^i $i = 1, \ldots, N_W$ are independent, identically distributed random variables with a probability density $p(\sigma_{th})$ and distribution function $P(\sigma_{th})$. For simplicity, we consider a uniform distribution between 0 and 1 so that $p(\sigma_{th})$ and $P(\sigma_{th})$ take the forms $p(\sigma_{th}) = 1$ and $P(\sigma_{th}) = \sigma_{th}$, respectively. The bundle is subject to a quasi-statically increasing external load σ parallel to the direction of fibers. When a fiber breaks in the bundle its load has to be shared by the remaining intact fibers. As a crucial element of the model, we assume that the load sharing is completely localized in the system so that the excess load after failure events is equally redistributed over the intact nearest neighbors of failed fibers. This localized load sharing (LLS) introduces spatial correlations in the system which makes it impossible to carry out analytical calculations. However, in the limit of equal load sharing (ELS) the most important characteristics of the fracture process can be obtained in closed analytical form.

Mean field solution

For the more realistic case of localized load redistribution our calculations showed that the presence of unbreakable fibers results in a broad spectrum of novel behaviors recovering also the classical LLS case in the $\alpha \to 0$ limit [2, 12, 25–29]. In the two-component mixture, the unbreakable fibers act as a load reservoir, i.e. the load they carry, especially the load increments they receive from their broken weak neighbors, doesn't contribute to the breaking process; from the viewpoint of breakable fibers this load is dissipated. It has the consequence that increasing the fraction of strong fibers reduces the stress concentration around failed regions. This way varying α we control the relative importance of stress concentration and disorder in the failure process, which is expected to have interesting consequences both on the micro and macro-scales.

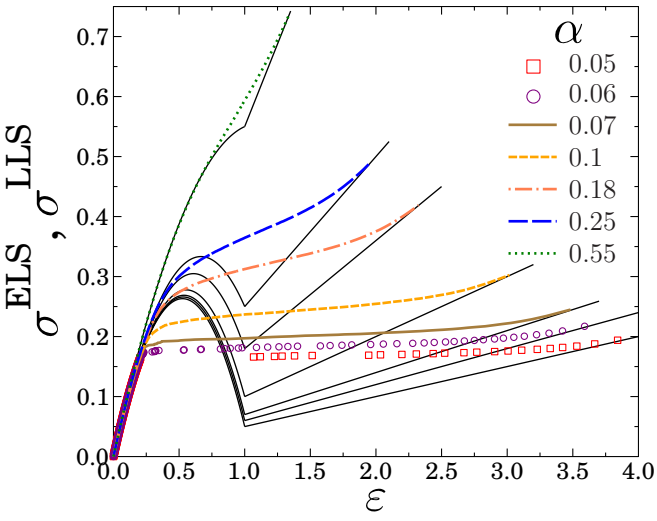

FIG. 1. *(Color online)* The constitutive behavior the two-component bundle for ELS (continuous lines) and *LLS* (dashed-dotted lines with different colors). The transition from brittle to ductile behaviour can clearly be observed as α increases.

In order to obtain a detailed understanding of the effect of stress localization on the fracture process of two-component mixtures, we carried out computer simulations on a square lattice of size $L = 401$ with periodic boundary conditions in both directions varying the value of α between 0 and 1. Averages were calculated over 100 samples with different realizations of disorder.

III. MACROSCOPIC RESPONSE

Figure 1 presents the constitutive curve of the *LLS* bundle $\sigma^{LLS}(\varepsilon)$ for several different values of α together with the corresponding ELS results $\sigma^{ELS}(\varepsilon)$. At $\alpha = 0$ when the system contains only breakable fibers we recover the former *LLS* results, namely, the *LLS* constitutive curve follows the ELS analytic solution [2, 12, 25–29]. However, the critical stress σ_c^{LLS} and strain ε_c^{LLS}, where macroscopic failure occurs, are significantly lower than the ELS values σ_c^{ELS} and ε_c^{ELS} falling in the linear regime of $\sigma(\varepsilon)$. The result implies that under *LLS* conditions FBMs exhibit a more brittle behaviour than for long range load redistribution. Under stress controlled loading macroscopic failure occurs in the form of a catastrophic avalanche at σ_c^{LLS} during which all remaining fibers break. For finite α values it can be observed in

Fig. 1 that the structure of $\sigma^{LLS}(\varepsilon)$ has two substantially different regimes: increasing the external load σ for α values close to zero the constitutive curve has a finite horizontal jump than it continues again along the ELS analytic solution. The discontinuity of $\sigma^{LLS}(\varepsilon)$ is the consequence of a major avalanche in which a macroscopic fraction of weak fibers breaks, however, not all of them. The short part of $\sigma^{LLS}(\varepsilon)$ converging to the asymptotic linear curve indicates that a small fraction of fibers survives and gradually breaks as the external load σ is further increased. It is important to emphasize that there exists a well defined value α_c of the control parameter at which the jump and the dominating avalanche disappears and $\sigma^{LLS}(\varepsilon)$ becomes a continuous monotonically increasing function. Increasing α above α_c the qualitative form of the constitutive curve does not change anymore. It is a very important feature of the system that in the regime $\alpha > \alpha_c$ the macroscopic response exhibits ductile behaviour, i.e. instead of catastrophic collapse observed below the critical point, the fracture process retains stability up to very large strain values.This brittle-ductile transition occurs at an astonishingly low fraction of strong fibers $\alpha_c^{LLS} \approx 0.059(5)$ compared to the corresponding mean-field counterpart $\alpha_c^{LLS} \ll \alpha_c^{ELS}$.

The unique macroscopic response of the system is the fingerprint of the special features of the microscopic fracture process. Due to the localized interaction of fibers, both spatial and temporal correlations arise at the microlevel: breaking fibers trigger bursts which are spatially localized and result in correlated growth of cracks. In order to characterize the breaking process on the micro scale, we analyze the statistics of bursts of simultaneously failing fibers and the spatial structure of broken clusters.

IV. BURST SIZE DISTRIBUTION

The failure process of *LLS* fiber bundles has recently been explored in details by computer simulations in the case of $\alpha = 0$ where the bundle is only composed of weak fibers [2, 12, 25–29]. It was found that under an increasing external load first the weakest fibers break in a random manner homogeneously dispersed over the entire system. As the external load increases the load dropped by the broken fibers becomes sufficient to result in additional breakings. This way breaking fibers can trigger avalanches of breaking events which are spatially correlated giving rise to growing clusters of broken elements. Connected clusters of broken fibers on the lattice can be interpreted as cracks in FBMs [26]. The microscopic origin of the brittle behaviour, observed in the limit of $\alpha = 0$ in Fig. 1, is that along the perimeter of growing cracks a high load is concentrated, which easily initiates a catastrophic avalanche already at crack sizes much smaller than the system size. As a consequence, in our simulations the completely weak system cannot tolerate large bursts and the size distribution $P(\Delta)$ becomes a

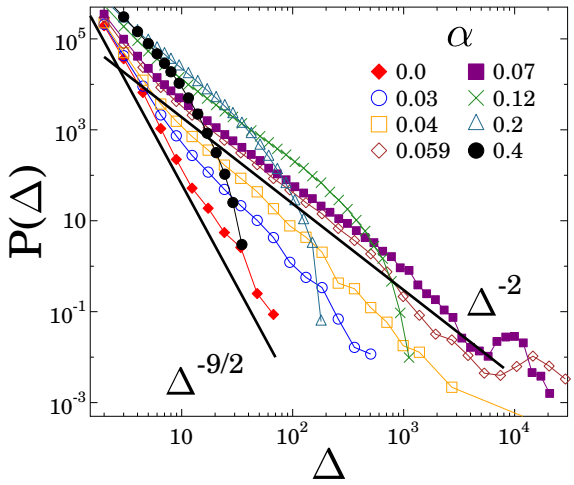

FIG. 2. *(Color online)* Avalanche size distributions $P(\Delta)$ at different values of α below and above α_c. Straight lines with slope 9/2 and 2.0 are drawn to guide the eye.

rapidly decreasing function. Our data analysis showed that the distribution function is a power law with a relatively large exponent (see Fig. 2)

$$P(\Delta) \sim \Delta^{-\mu}, \qquad \text{where} \qquad \mu \approx 9/2, \tag{1}$$

in agreement with former predictions [25, 26, 29]. For increasing α simulations revealed that the reduction of stress concentration by strong fibers allows the system for larger avalanches. It can be observed in Fig. 2 that the exponent $\mu \approx 9/2$ remains for small avalanche sizes, while for large avalanches a crossover occurs to a lower exponent $\mu \approx 2.0$. Approaching the critical value α_c, the second power law regime spans over nearly three orders of magnitude in a system of size $L = 401$. Note the bump of $P(\Delta)$ for the largest avalanches. Since the largest avalanche of the system is always followed by a few small ones, no catastrophic avalanche can be identified in the sense of simple FBMs obtained in the $\alpha = 0$ limit. Hence, all the avalanches were accumulated in the statistics so that the largest avalanches form a bump of Gaussian shape on the total distribution.

It can be seen in Fig. 2 that above α_c the bump of large avalanches disappears and $P(\Delta)$ develops an exponential cutoff. Increasing α the cutoff burst size decreases, however, the exponent of the power law regime remains constant. Scaling analysis revealed that rescaling the two axis by appropriate powers of a characteristic avalanche size, the distributions $P(\Delta)$ above the critical point α_c can be collapsed onto a master curve. Using the average size of the largest avalanche $\overline{\Delta}_{max}$ as scaling variable, an excellent quality data collapse is obtained in Fig. 3 which implies the scaling structure of the burst size distribution

$$P(\Delta) = \overline{\Delta}_{max}^{-\beta} f(\Delta/\overline{\Delta}_{max}^{\xi}), \qquad \text{for} \qquad \alpha > \alpha_c. \tag{2}$$

Best collapse was achieved in Fig. 3 with the exponents $\xi = 1.24$ and $\beta = 2.5$. It is important to emphasize that

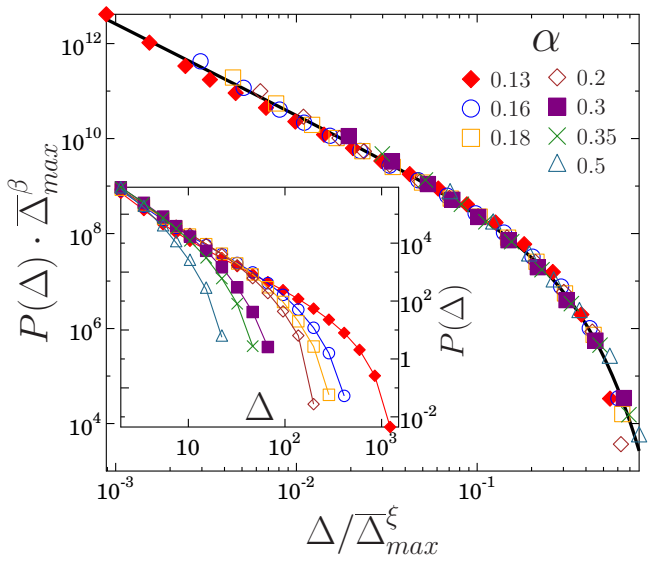

FIG. 3. *(Color online)* Scaling plot of avalanche size distributions above α_c using the average size of the largest avalanche $\overline{\Delta}_{max}$ as scaling variable. An excellent collapse is achieved with the exponents $\xi = 1.24$ and $\beta = 2.5$. The bold line represents the fit with Eq. (3), where $\mu = 1.97$ was obtained. The original distributions $P(\Delta)$ are presented in the inset.

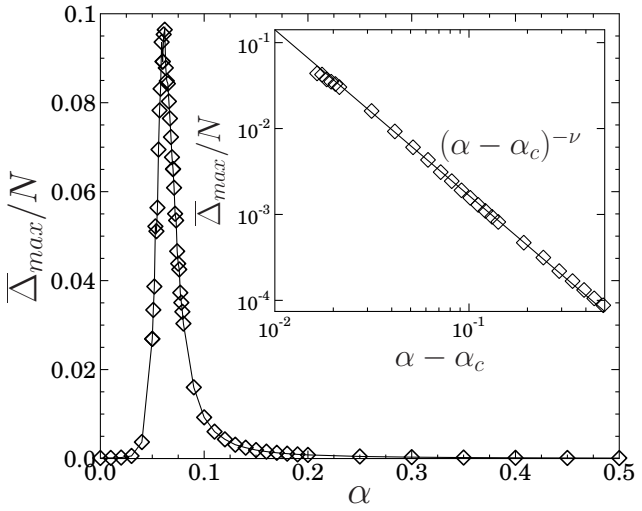

FIG. 4. Average size of the largest avalanche $\overline{\Delta}_{max}$ as a function of α. The position of the sharp peak α_c coincides with the critical value of α we identified based on the constitutive curves. Inset: the same quantity plotted as a function of the distance from the critical point $\alpha-\alpha_c$. A straight line of slope 1.95 is drawn to guide the eye.

the scaling function f has the functional form

$$f(\Delta/\overline{\Delta}_{max}^{\xi}) \sim \Delta^{-\mu}\exp\left(-\Delta/\overline{\Delta}_{max}^{\xi}\right), \qquad (3)$$

i.e., it can be described as a power law followed by an exponential cutoff. The value of the exponent was obtained by fitting as $\mu = 2.0 \pm 0.05$. Note that due to the condition of normalization the three exponents ξ, β, and μ must fullfill the scaling relation $\beta = \xi\mu$. Substituting the numerical values good agreement can be found. The above scaling analysis also demonstrates that the value of the exponent μ of the burst size distribution is constant above the critical point so that any apparent change of μ in Fig. 3 can be attributed to the moving cutoff.

Computer simulations showed that the characteristic avalanche size $\overline{\Delta}_{max}$ as a function of α has a sharp peak (see Fig. 4) at the same α_c which has been defined based on the constitutive curve of the system in Fig. 1. Replotting $\overline{\Delta}_{max}$ as a function of $\alpha-\alpha_c$ in the inset of Fig. 4 a straight line is obtained on a double logarithmic plot which implies the power law form

$$\overline{\Delta}_{max} \sim (\alpha-\alpha_c)^{-\nu}, \qquad \text{for} \qquad \alpha > \alpha_c. \qquad (4)$$

The value of the correlation length exponent ν was obtained numerically as $\nu = 1.95 \pm 0.07$. The result shows that approaching the critical point α_c from above the characteristic avalanche size has a power law divergence. When α is increased starting from zero, during the damaging of the bundle an increasing fraction of load is kept by the strong fibers which becomes inaccessible for the failure process. Since the active load decreases, the bundle can survive larger avalanches which finally at the critical point reach the scale of the system size. Comparing to the mean field solution of the model [30], it has to be noted that the burst size exponent μ of the regime $\alpha \geq \alpha_c$ is smaller, while the correlation length exponent ν is larger when the stress redistribution is localized. In Ref. [11] we have shown by analytical means that the burst size exponent of FBMs takes the value $\mu = 2$ when the constitutive curve has a long plateau preceded by an increasing regime with only a slight non-linearity. Our numerical results obtained for two-component mixtures is in perfect agreement with the analytical predictions of Ref. [11].

V. MICROSTRUCTURE OF DAMAGE

Contrary to equal load sharing, under *LLS* conditions fibers breaking in a burst form a connected set which may be part of a more extended cluster of broken fibers generated by previous avalanches. This way the cluster structure and the avalanches of breaking fibres become correlated. In the following we explore how the microstructure of damage evolves under an increasing external load σ for different compositions of the system and establish the relation of crack growth and breaking avalanches.

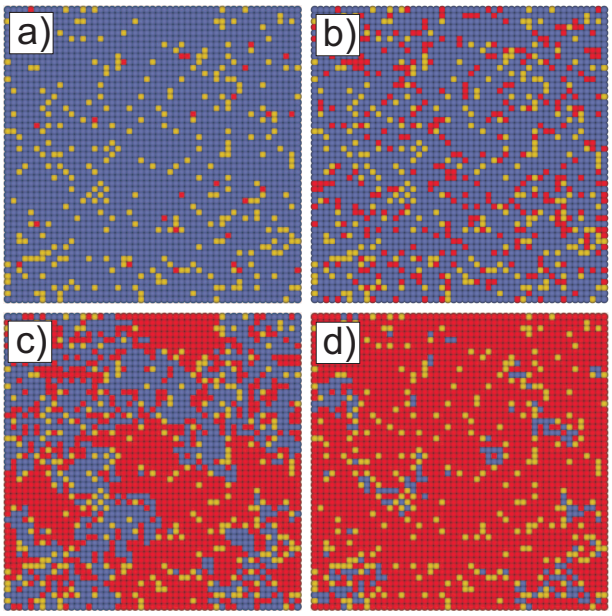

FIG. 5. *(Color online)* Snapshots of a damaging bundle of size $L = 50$ at four values of ε during the loading process with $\alpha = 0.07$. Blue and yellow colors represent intact weak and strong fibers, respectively, while red stands for the broken ones.

A. Nucleation, growth, and merging of cracks

It has been discussed that in the limit of $\alpha = 0$ all clusters of broken fibers are small compared to the system size and they are randomly dispersed over the entire bundle. Macroscopic failure is typically driven by the breaking of a single fiber which is located along the boundary of a larger cluster where the stress concentration is high [5, 17, 26, 31, 32]. However, at finite values of α the presence of strong fibers substantially influences the cluster structure of broken fibers of the weak component: strong fibers decrease the load transfered to the weak ones after breaking events which reduce the stress concentration around failed regions. As a consequence, at low values of α strong fibers let the system grow larger avalanches, and hence, more extended clusters of broken fibers can occur. However, at high α, strong fibers develop a counter effect, i.e. the load transfered to weak fibers after failure events will be so much reduced that it limits the propagating bursts and growing clusters. Since at a given value of α the bundle is a random mixture of weak and strong fibers, the underlying structural disorder of the mixture has also an additional effect. For the two-component system a direct mapping can be established to percolation lattices where $p_s = \alpha$ and $p_w = 1 - \alpha$ are the occupation probabilities of strong and weak fibers, respectively, with $p_s + p_w = 1$. Until α is small, i.e., until $p_s \leq p_c$ and $p_w \geq p_c$ hold, where $p_c \approx 0.5926$ is the critical occupation probability of site percolation on a square lattice [33], there exists a dominating cluster of weak fibers (spanning cluster) together with some additional clusters which are orders of magnitude smaller. However, for $\alpha > p_c$ the strong fibers form a spanning cluster, while all weak clusters are small. The intermediate regime $(1 - p_c) < \alpha < p_c$ is also interesting because here none of the components have a spanning cluster since $p_w < p_c$ and $p_s < p_c$ hold.

Figure 5 presents an example for the evolution of the cluster structure of the system for an increasing load σ (for demonstration purposes a relatively small lattice $L = 50$ is considered). It can be seen in Fig. 5(a) that as the external load σ is increased broken clusters grow which are scattered randomly over the entire lattice. In the example $\alpha = 0.07$ which is slightly above the critical point α_c, hence, clusters become so large that they can also merge (see Fig. 5(b, c)). Finally, in Fig. 5(d) nearly all weak fibers are broken so that cracks are identical with the clusters of the underlying weak component. In order to give a quantitative characterization of the evolution of the microstructure of damage we determined the average size $\langle S_{av} \rangle$ and the average number $\langle n_c \rangle$ of clusters of broken fibers as a function of the deformation ε during the loading process. In one sample the average cluster size S_{av} is defined as the ratio of the second and first moments of cluster sizes S_i

$$S_{av} = \frac{\sum_i S_i^2}{\sum_i S_i}, \tag{5}$$

where the largest cluster is always omitted in the summation. Then $\langle S_{av} \rangle (\varepsilon)$ is obtained by averaging S_{av} over a large number of samples at the same deformation ε. It can be observed in Fig. 6(a) that in the brittle regime $\alpha < \alpha_c$ the average cluster size $\langle S_{av} \rangle (\varepsilon)$ has only an increasing branch which suddenly stops at the instance of failure. However, in the ductile phase the $\langle S_{av} \rangle$ curves have a maximum followed by a rapidly decreasing part. Above the critical point $\alpha > \alpha_c$ the coalescence of cracks results in a macroscopic cluster which spans the entire system. The maximum of the curves $\langle S_{av} \rangle$ marks the configuration where the dominating cluster occurs. Since the largest cluster is always removed from the statistics, in the presence of a dominating cluster $\langle S_{av} \rangle$ must decrease. The situation drastically changes when α surpasses the value of $\alpha^* = 1 - p_c \approx 0.4077$ because in the regime $\alpha > \alpha^*$ the weak component does not have a spanning cluster and hence no dominating crack can emerge. Consequently, in this regime $\langle S_{av} \rangle$ monotonically increases and saturates when nearly all weak fibers break.

It can be observed in Fig. 6(a) that the maximum value $\langle S_{av} \rangle^{max}$ shows also an interesting systematics as the composition α of the system is changed. For clarity, we also present separately the maximum $\langle S_{av} \rangle^{max}$ as a function of α in Fig. 7. In the brittle phase $\alpha < \alpha_c$ the maximum $\langle S_{av} \rangle^{max}$ is simply the value of the terminal point of the function $\langle S_{av} \rangle (\varepsilon)$ at the instant of failure which is practically independent of α. However, as α surpasses the critical point α_c the coalescence results in crack sizes which are orders of magnitude larger than the

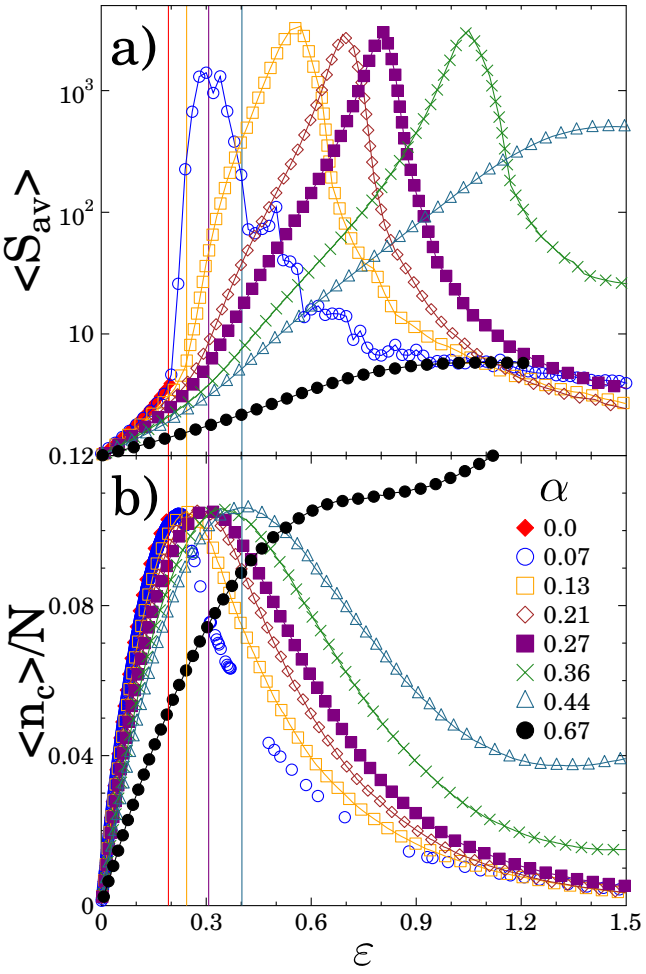

FIG. 6. *(Color online)* Average cluster size $\langle S_{av}\rangle$ (a) and average number of clusters $\langle n_c\rangle$ (b) as function of ε for several compositions α of the system. For clarity, the vertical straight lines indicate the position ε_m^{nc} of the maximum of $\langle n_c\rangle$ for a few α values. The color of these lines corresponds to the color code of the data sets in (a) and (b).

brittle ones. Inside the ductile regime $\alpha > \alpha_c$ the maximum remains constant since it is only determined by the system size N until the weak fibers have a spanning cluster $\alpha_c \leq \alpha \leq \alpha^*$. However, for $\alpha > \alpha^*$ the maximum of $\langle S_{av}\rangle(\varepsilon)$ is reached at saturation, when all the weak clusters have been broken. Hence, in this regime the maximum value $\langle S_{av}\rangle^{max}$ is a decreasing function of α in Fig. 7. It is interesting to note that approaching α^* from above $\alpha \to \alpha_+^*$ the occupation probability of the weak component $p_W = 1-\alpha$ tends to p_c from below. It has the consequence that the maximum value of the average crack size $\langle S_{av}\rangle^{max}$ in the regime $\alpha > \alpha^*$ has the same critical behaviour as the average cluster size of percolation when approaching the critical point

$$\langle S_{av}\rangle^{max} \sim (p_c - p_w)^{-\gamma}. \tag{6}$$

The inset of Fig. 7 demonstrates that the above prediction is perfectly fullfilled by the simulation data. The numerical value of the exponent $\gamma = 2.33 \pm 0.08$ falls very close to the corresponding exponent of percolation $\gamma = 43/18 \approx 2.39$ [33].

The average number of cracks $\langle n_c\rangle$ also encodes interesting information about the evolution of the crack ensemble. It can be observed in Fig. 6(b) that in the brittle regime $\alpha < \alpha_c$ the number of cracks monotonically increases and stops suddenly due to the abrupt failure of the system (compare to Fig. 1). When the fracture is ductile $\alpha \geq \alpha_c$ the $\langle n_c\rangle$ curves develop a decreasing regime due to the coalescence of cracks such that the position of the maximum ε_m^{nc} marks the configuration where coalescence starts. For clarity, the maximum position ε_m^{nc} is indicated by the vertical lines in Fig. 6 for a few α values. Comparing Fig. 6(a) and Fig. 6(b) it can be observed that at ε_m^{nc} the average cluster size switches to a faster increase reaching its maximum at a deformation ε_m^S larger than ε_m^{nc}. Note that for $\alpha < \alpha_c$ the value of ε_m^S coincides with ε_m^{nc} and also with ε_c^{LLS} where macroscopic failure occurs. For larger α the inequality

$$\varepsilon_m^{nc} < \varepsilon_m^S \tag{7}$$

holds. Only those cracks can merge which grew inside larger clusters of the weak component. Small isolated weak clusters break only at higher load values due to the strong load reduction of the strong ones. This explains why in Fig. 6(b) the merging regime of $\langle n_c\rangle$ is followed by a short increase (see e.g. the curve of $\alpha = 0.44$ in Fig. 6(b)). It is important to emphasize that the decreasing branch of $\langle n_c\rangle$ prevails even above α^*, which shows that merging can occur not only inside the spanning cluster, but even smaller weak clusters may develop several cracks which later on merge.

The most remarkable result is that the maximum value of the cluster number remains constant $\langle n_c\rangle/N \approx 0.1$ until the strong component does not have a spanning cluster $\alpha < p_c$. In this parameter regime the maximum cluster number is determined solely by the disorder of the breaking thresholds of weak fibers and by the system size. Our result indicates that for uniformly distributed breaking thresholds approximately 10% of the lattice sites serve as nucleation centers of cracks. Until $\alpha < p_c$ the presence of strong fibers only influences the value of the deformation ε_m^{nc} where the maximum is reached. The disappearance of merging is indicated by the monotonicity of $\langle n_c\rangle$ which occurs when α exceeds p_c. In this regime strong fibers have a spanning cluster and the weak clusters get so small that in each of them practically one crack nucleates which gradually covers the entire cluster.

In order to quantify the effect of strong fibers on the evolution of the number of cracks during the loading process, in Fig. 8(a) we replotted the $\langle n_c\rangle/N$ curves as a function of $\varepsilon(1-\alpha)$. A high quality data collapse is obtained up to the maximum. The result implies that during the loading process of the bundle crack nucleation

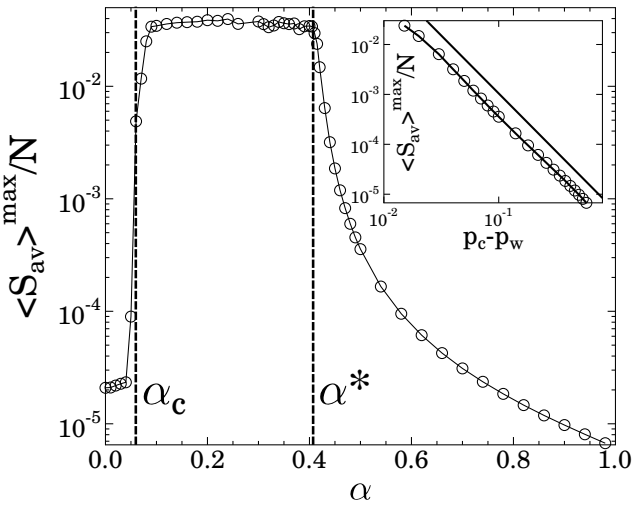

FIG. 7. The maximum value of the average cluster size $\langle S_{av}\rangle^{max}$ averaged over a large number of samples at a given α. Three distrinct regimes can clearly be distinguished which are separated by α_c and α^*. The inset presents the same quantity in the range $\alpha > \alpha^*$ as a function of $p_c - p_W$, where $p_W = 1 - \alpha$. The straight line has slope 2.32.

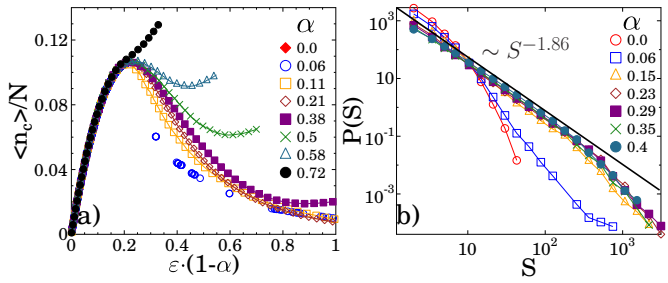

FIG. 8. *(Color online)* (*a*) Average number of cracks as a function of ε rescaled along the horizontal axis with $p_w = 1 - \alpha$. High quality data collapse can be observed up to the maximum. (*b*) Cluster size distributions determined at ε_m^S for several compositions α.

dominates up to deformations

$$\varepsilon_m^{nc} \sim \frac{1}{1-\alpha}, \tag{8}$$

while beyond ε_m^{nc} merging of cracks governs the evolution of the microstructure. It also follows that large bursts of breaking fibers are generated in the $\varepsilon > \varepsilon_m^{nc}$ regime of the constitutive curves $\sigma(\varepsilon)$ and they are mainly growth steps of existing cracks. The situation changes for $\alpha > p_c$ because strong fibers prevent merging of cracks nucleated in isolated weak clusters. In this case cracks must nucleate even for $\varepsilon > \varepsilon_m^{nc}$ to break all weak fibers, and hence, $\langle n_c\rangle$ becomes monotonically increasing.

B. Size distribution of cracks

It is an interesting question about fracture phenomena how the size distribution of cracks behaves at failure or at the point of localization [17, 26, 34–36]. In the brittle phase $\alpha < \alpha_c$ of our FBM we evaluated the size distribution of cracks in the last stable configuration of the bundle before the catastrophic avalanche. It has been discussed above that in the ductile phase $\alpha > \alpha_c$ the onset of localization is marked by the position of the maximum ε_m^{nc} of the number of cracks. However, the crack structure at this deformation is rather close to the critical configuration of the $\alpha = 0$ completely weak system. That's why the size distribution of cracks $P(S)$ was evaluated at the deformation ε_m^S where the average cluster size $\langle S_{av}\rangle(\varepsilon)$ has its maximum.

Figure 9 presents the configuration of the bundle at ε_m^S for several values of α. It can be observed in Fig. 9(*a*) that if the bundle only contains weak fibers $\alpha = 0$ all clusters are small compared to the system size. Consquently, in Fig. 8(*b*) the corresponding size distribution $P(S)$ is a rapidly decreasing exponential in agreement with former results on LLS FBMs [5, 17, 26]. In the ductile regime $\alpha > \alpha_c$ the spanning cluster covers a large fraction of the system (see Fig. 9(*b, c, d*)), however, the size of smaller cracks scatter over a broad interval, as well. It is important to note that in these cases the cluster size distribution has a power law regime

$$P(S) \sim S^{-\tau}, \tag{9}$$

followed by an exponential cutoff. The value of the exponent $\tau = 1.86 \pm 0.05$ proved to be lower than the corresponding exponent of percolation $\tau = 187/91 \approx 2.05$ [33]. It shows that larger cracks more frequently occur due to the correlated growth mechanism and coalescence. It is interesting to note that our results on the size distribution of cracks have a good agreement with Ref. [34], where a two dimensional fracture model predicted power law distributed crack sizes with exponent 2. The authors argued that the growth and coalescence of cracks along the softening regime of the constitutive curve are responsible for the scale free distribution. However, when the failure is brittle or quasi-brittle exponential or lognormal distributions have been obtained in various types of fracture models [17, 26, 35, 37] again in agreement with our results.

VI. DISCUSSION

We investigated the fracture process of highly heterogeneous materials in the framework of a fiber bundle model. The fibers have identical elastic properties, however, their fracture characteristics are strongly different: a fraction of fibers is strong in the sense that they can sustain any load without breaking, while the rest of fibers is weak having statistically distributed strength

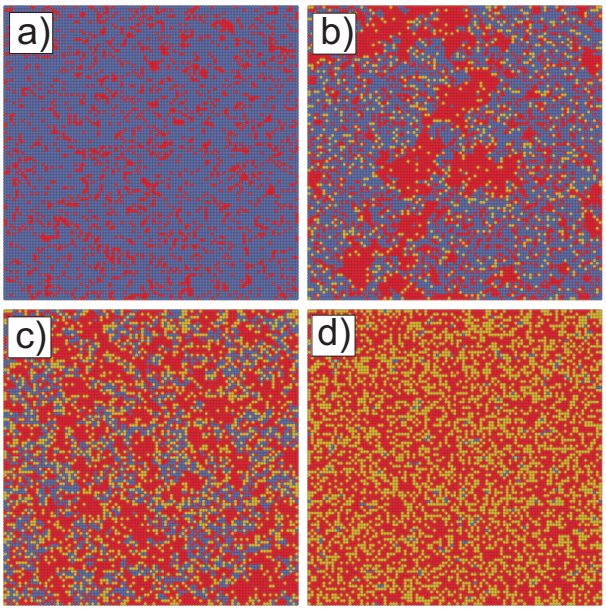

FIG. 9. *(Color online)* Snapshots of the cluster structure in systems of size $L = 100$ taken at the deformation ε_m^S where the average cluster size $\langle S_{av} \rangle$ has a maximum for different values of the control parameter α: (a) 0 (b) 0.08 (c) 0.35 (d) 0.4. When the system only contains weak fibers (a) all the clusters are small compared to the system size. Above the critical point α_c growth and merging result in large cluster sizes which are only limited by the system size and by the underlying lattice structure of the weak and strong components.

values. The two components are homogeneously mixed on a square lattice which is then loaded in a stress controlled way. In order to capture the effect of stress concentration around cracks, we considered localized load sharing such that the load of broken fibers is redistributed equally over its intact nearest neighbors on the lattice. Our computer simulations revealed that varying the fraction of strong fibers α as a control parameter the system exhibits a very interesting behaviour with several novel aspects.

Investigating the macroscopic constitutive behaviour of the system we pointed out that at a critical value α_c a transition occurs from highly brittle to ductile response. The brittle phase is characterized by the presence of an instable branch of the constitutive curve along which a macroscopic fraction of fibers breaks in a catastrophic avalanche when performing stress controlled loading. In the ductile regime the constitutive curve is monotonous which implies stable fracture gradually breaking the weak component in finite avalanches. The critical fraction has an astonishingly small value showing that adding a very small amount of strong fibers can be sufficient to stabilize an originally brittle system.

On the microscopic scale our simulations revealed that the interplay of the inhomogeneous stress field arising due to the localized load redistribution and of the load-absorbing effect of strong fibers leads to a rich dynamics. In the ductile regime the size distribution of avalanches proved to be a power law with an exponent $\mu = 2.0$, which is significantly lower than the one of the brittle phase $\mu = 9/2$. Approaching the critical fraction from above, the characteristic size of breaking avalanches has a power law divergence which showes that the brittle-ductile transition occurs analogous to continuous phase transitions.

The localized load redistribution has the consequence that avalanches of fiber breakings form spatially connected clusters. Since high stress is concentrated along the perimeter of broken clusters, avalanches are typically triggered at these fibers so that avalanches are intermittent steps of the growth of cracks. Our investigations showed that in the brittle regime only small cracks can develop compared to the system size. However, in the ductile phase the load absorbed by the strong fibers allows the cracks to reach sizes where they merge and form a macroscopic crack spanning the entire system. Merging always occurs until it becomes prevented by the spanning cluster of the strong component in the limit of large values of the controll parameter α.

Analysing the statistics of bursts and cracks, we pointed out that at the beginning of the loading process the nucleation of cracks dominates, while later on coalescence governs the evolution of the microstructure. Since the maximum number of cracks does not change, bursts emerging along the plateau of the constitutive curve in the ductile regime are steps of stable crack propagation.

ACKNOWLEDGMENTS

The work is supported by TAMOP-4.2.1/B-09/1/KONV-2010-0007 and by TAMOP-4.2.2/B-10/1-2010-0024 projects. The project is implemented through the New Hungary Development Plan, co-financed by the European Union, the European Social Fund and the European Regional Development Fund. F. Kun acknowledges the support of OTKA K84157. This work was supported by the European Commissions by the Complexity-NET pilot project LOCAT.

[1] M. Alava, P. K. Nukala, and S. Zapperi, Adv. in Phys. **55**, 349476 (2006).
[2] S. Pradhan, A. Hansen, and B. K. Chakrabarti, Reviews of Modern Physics **82**, 499 (2010).
[3] S. Pradhan, B. K. Chakrabarti, and A. Hansen, Phys. Rev. E **71**, 036149 (2005).
[4] R. C. Hidalgo, F. Kun, and H. J. Herrmann, Phys. Rev. E **64**, 066122 (2001).

[5] R. C. Hidalgo, Y. Moreno, F. Kun, and H. J. Herrmann, Phys. Rev. E **65**, 046148 (2002).
[6] G. G. Batrouni and A. Hansen, Phys. Rev. Lett. **80**, 325 (1998).
[7] P. V. V. Nukala, S. Simunovic, and S. Zapperi, J. Stat. Mech: Theor. Exp., P08001(2004).
[8] G. A. D'Addetta, F. Kun, and E. Ramm, Gran. Matt. **4**, 77 (2002).
[9] F. Raischel, F. Kun, and H. J. Herrmann, Phys. Rev. E **72**, 046126 (2005).
[10] P. K. V. V. Nukala, P. Barai, S. Zapperi, M. J. Alava, and S. Scaronimunovicacute, Phys. Rev. E **82**, 026103 (2010).
[11] R. C. Hidalgo, F. Kun, K. Kovács, and I. Pagonabarraga, Phys. Rev. E **80**, 051108 (2009).
[12] M. Kloster, A. Hansen, and P. C. Hemmer, Phys. Rev. E **56**, 26152625 (1997).
[13] F. Kun, H. A. Carmona, J. S. A. Jr, and H. J. Herrmann, Phys. Rev. Lett. **100**, 094301 (2008).
[14] A. Saichev and D. Sornette, Phys. Rev. E **71**, 016608 (2005).
[15] J. V. Andersen, D. Sornette, and K. Leung, Phys. Rev. Lett. **78**, 21402143 (1997).
[16] S. Zapperi, A. Vespignani, and H. E. Stanley, Nature **388**, 658 (1997).
[17] S. Zapperi, P. Ray, H. E. Stanley, and A. Vespignani, Phys. Rev. Lett. **78**, 1408 (1997).
[18] Y. Moreno, J. B. Gomez, and A. F. Pacheco, Phys. Rev. Lett. **85**, 2865 (2000).
[19] K. Kovács, S. Nagy, F. Kun, H. J. Herrmann, and I. Pagonabarraga, Phys. Rev. E **77**, 036102 (2008).
[20] F. L. Matthews and R. D. Rawlings, *Composite Materials: Engineering and Science*, 1st ed. (Chapman & Hall, London, 1994).
[21] D. Amitrano, J. Geophys. Res. **108**, 2044 (2003).
[22] C. B. Picallo, J. M. López, S. Zapperi, and M. J. Alava, Phys. Rev. Lett. **105**, 155502 (2010).
[23] F. Raischel, F. Kun, and H. J. Herrmann, Phys. Rev. E **73**, 066101 (2006).
[24] D. Krajcinovic, *Damage Mechanics* (North Holland, Amsterdam, 1996).
[25] A. Hansen and P. C. Hemmer, Phys. Lett. A **184**, 394396 (1994).
[26] F. Kun, S. Zapperi, and H. J. Herrmann, Eur. Phys. J. B **17**, 269 (2000).
[27] W. I. Newman and S. L. Phoenix, Phys. Rev. E **63**, 021507 (2001).
[28] S. L. Phoenix and W. I. Newman, Phys. Rev. E **80**, 066115 (2009).
[29] F. Raischel, F. Kun, and H. J. Herrmann, Phys. Rev. E **74**, 035104 (2006).
[30] R. C. Hidalgo, K. Kovács, I. Pagonabarraga, and F. Kun, Europhys. Lett. **81**, 54005 (2008).
[31] S. Zapperi, P. Ray, H. E. Stanley, and A. Vespignani, Phys. Rev. E **59**, 5049 (1999).
[32] F. Bosia, M. J. Buehler, and N. M. Pugno, Phys. Rev. E **82**, 056103 (2010).
[33] D. Stauffer and A. Aharony, *Introduction to Percolation Theory* (Taylor & Francis, 1992).
[34] C. Spyropoulos, C. H. Scholz, and B. E. Shaw, Phys. Rev. E **65**, 056105 (2002).
[35] S. Nukala, P. K. V. V. Nukala, S. Šimunović, and F. Guess, Phys. Rev. E **73**, 036109 (2006).
[36] K. Z. Nanjo and D. L. Turcotte, Geophys. J. Int. **162**, 859 (2005).
[37] A. Stormo, K. S. Gjerden, and A. Hansen, Phys. Rev. E **86**, 025101 (2012).